Bi-Level Volt-VAR Optimization to Coordinate Smart Inverters With Voltage Control Devices

Rahul Ranjan Jha, *Student Member, IEEE*, Anamika Dubey, *Member, IEEE*, Chen-Ching Liu, *Fellow, IEEE*, and Kevin P. Schneider, *Senior Member, IEEE*

***Abstract*—Conservation voltage reduction (CVR) uses Volt-VAR optimization (VVO) methods to reduce customer power demand by controlling feeder's voltage control devices. The objective of this paper is to present a VVO approach that controls system's legacy voltage control devices and coordinates their operation with smart inverter control. An optimal power flow (OPF) formulation is proposed by developing linear and nonlinear power flow approximations for a three-phase unbalanced electric power distribution system. A bi-level VVO approach is proposed, where Level 1 optimizes the control of legacy devices and smart inverters using a linear approximate three-phase power flow. In Level 2, the control parameters for smart inverters are adjusted to obtain an optimal and feasible solution by solving the approximate nonlinear OPF model. Level 1 is modeled as a mixed integer linear program (MILP) while Level 2 as a nonlinear program with linear objective and quadratic constraints. The proposed approach is validated using 13-bus and 123-bus three-phase IEEE test feeders and a 329-bus three-phase PNNL taxonomy feeder. The results demonstrate the applicability of the framework in achieving the CVR objective. It is demonstrated that the proposed coordinated control approach help us to reduce the feeder's power demand by reducing the bus voltages; the proposed approach maintains an average feeder voltage of 0.96 p.u. A higher energy saving is reported during the minimum load conditions. The results and approximation steps are thoroughly validated using OpenDSS.**

***Index Terms*—Volt-VAR optimization, smart inverters, distributed generators, three-phase optimal power flow.**

NOMENCLATURE

Sets

$\mathcal{G} = (\mathcal{N}, \mathcal{E})$	Directed graph for distribution system
$\mathcal{E}$	Set of distribution lines (branches) in G
$\mathcal{E}_{\mathcal{T}}$	Set of branches with voltage regulator
$\mathcal{N}$	Set of buses (nodes) in G
$\mathcal{N}_{\mathcal{C}}$	Set of nodes with capacitor banks
$\mathcal{N}_{\mathcal{DG}}$	Set of nodes with smart inverter connected DGs
Φ_i	Set of phases of bus i where, $\Phi_i \subseteq \{a, b, c\}$
Φ_{ij}	$\{(pq) : p \in \Phi_i, q \in \Phi_j\}$

Variables

(i, j)	Line(branch) connecting nodes i and j
I_{ij}^p	$I_{ij}^p = \lvert I_{ij}^p \rvert \angle \delta_{ij}^p$ is complex line current corresponding to phase $p \in \Phi_i$ where, $\lvert I_{ij}^p \rvert$ is magnitude and δ_{ij}^p is corresponding phase angle.
$p_{DG,i}^p$	Projected per-phase active power generated by i^{th} DG at the current time instance.
$q_{DG,i}^p$	Available per-phase reactive power from i^{th} DG at the current time instance.
$q_{cap,i}^{rated,p}$	Rated reactive power generated by capacitor bank connected to phase p of bus i
s	Substation bus where, $s \in \mathcal{N}$
$s_{DG,i}^{rated,p}$	Rated per-phase apparent power capacity for DG connected to bus $i \in \mathcal{N}_{\mathcal{DG}}$
$s_{L,i}^p$	$s_{L,i}^p = p_{L,i}^p + j q_{L,i}^p$ is complex power demand at bus i corresponding to phase $p \in \Phi_i$ where, $p_{L,i}^p$ and $q_{L,i}^p$ are corresponding active and reactive power demand, respectively.
S_{ij}^{pq}	$S_{ij}^{pq} = P_{ij}^{pq} + j Q_{ij}^{pq}$ is complex power flow in branch (i, j) corresponding to $(pq) \in \Phi_{ij}$, where, P_{ij}^{pq} and Q_{ij}^{pq} are corresponding active and reactive components, respectively.
$u_{tap,i}^p$	Binary control variable for voltage regulator tap position connected to phase p of bus i
$u_{cap,i}^p$	Binary control variable for capacitor bank connected to phase p of bus i where, $i \in \mathcal{N}_{\mathcal{C}}$
V_i^p	$V_i^p = \lvert V_i^p \rvert \angle \theta_i^p$ is complex voltage for $p \in \Phi_i$
z_{ij}	Complex three-phase impedance matrix for line $(i, j) \in \mathcal{E}$
z_{ij}^{pq}	$z_{ij}^{pq} = r_{ij}^{pq} + j x_{ij}^{pq}$ is an element of the complex impedance matrix z_{ij} for branch (i, j) where, $(pq) \in \Phi_{ij}$

Manuscript received February 11, 2018; revised July 16, 2018 and October 5, 2018; accepted December 15, 2018. Date of publication January 1, 2019; date of current version April 17, 2019. This work was supported in part by the U.S. Department of Energy under contract DE-AC05-76RL01830. Paper no. TPWRS-00204-2018. *(Corresponding author: Anamika Dubey.)*

R. R. Jha, A. Dubey, and C.-C. Liu are with the School of Electrical Engineering and Computer Science, Washington State University, Pullman, WA 99164 USA (e-mail: rahul.jha@wsu.edu; anamika.dubey@wsu.edu; liu@eecs.wsu.edu).

K. P. Schneider is with the Pacific Northwest National Laboratory, Battelle Seattle Research Center, Seattle, WA 98109 USA (e-mail: kevin.schneider@pnnl.gov).

Color versions of one or more of the figures in this paper are available online at http://ieeexplore.ieee.org.

Digital Object Identifier 10.1109/TPWRS.2018.2890613

I. INTRODUCTION

CONSERVATION voltage reduction (CVR) is a technology to increase the energy efficiency of electric power distribution systems by reducing customer power demand through voltage control. The benefits of voltage control to energy savings are realized due to the sensitivity of customer loads to

service voltages where decreasing the voltage helps reduce the demand [1], [2]. Based on several studies and pilot projects, CVR can help achieve attractive energy savings. In fact, a recent study shows that CVR can help reduce the annual energy consumption by 3.04% when implemented on all distribution feeders throughout the United States [1].

Traditionally, CVR is accomplished by controlling feeder's legacy voltage control devices such as capacitor banks, load tap changers, and voltage regulators using Volt-VAR control (VVC) techniques. The feeder is operated at a lower service voltage range while still maintaining the service voltages within the recommended ANSI voltage limits (0.95–1.05 pu) [3]. In literature, several VVC methods have been proposed: 1) using autonomous or rule-based approach, 2) based on end-of-line measurements and 3) using integrated Volt-Var Control (IVVC) based on real-time measurements [4]–[6]. Several commercial VVC products are also available that perform IVVC function mostly using heuristic [7]. Unfortunately, the available products only optimize the operation of legacy control devices. Recently, the integration of distributed generation (DGs) has increased in the distribution grid [8]. Most DGs are equipped with smart inverters that are capable of absorbing and supplying reactive power and thus controlling the feeder voltages locally that can help achieve additional CVR benefits [9]. Several researchers have worked on optimizing the reactive power dispatch from DGs and have proposed methods for smart inverter control using: 1) autonomous control, 2) distributed control, and 3) centralized control using optimal power flow (OPF) [10]–[14].

The existing literature, however, presents several limitations. First, the available literature mostly fails to coordinate the control of feeder's legacy devices with smart inverters connected to DG. When mathematically modeling the VVO problem for both legacy and new devices, the optimization requires solving an OPF problem with both discrete and continuous variables. This results in a Mixed Integer Nonlinear Program (MINLP) that includes power flow equations for a three-phase unbalanced system. Some recent articles attempt to solve this problem [15]–[21]. Unfortunately, these methods do not jointly optimize the control of legacy devices and new devices, do not apply to three-phase unbalanced system, or do not scale well even for mid-size system as the underlying problem is a MINLP. Second, the methods based on OPF assume a constant power load model thus fail to incorporate the voltage dependency of customer loads that is critical for modeling CVR effects. A voltage-dependent load model that can be easily incorporated within the optimization framework is called for. Third, the existing literature mostly solves a single-phase OPF problem. Distribution systems are largely unbalanced and require complete three-phase modeling to deliver a reasonable result. Recently, there has been some advancements in solving three-phase OPF problem, however, due to associated nonlinearities and mutual couplings, solving a three-phase OPF with only continuous decision variables is a challenging problem [22], [23]. Introducing discrete variables to three-phase OPF problem makes it even more challenging to solve. The aforementioned gap in literature calls for further research on enabling CVR for a modern distribution system. The objective of this paper to develop an OPF based bi-level approach for VVO to achieve CVR benefits for a three-phase unbalanced radial distribution system by simultaneously controlling both legacy devices and smart inverters. The proposed approach aims at addressing the aforementioned gaps in the literature and presents a scalable model for coordinated control of grid's all voltage control devices for CVR benefits. First, models for voltage-dependent loads and systems voltage control devices are developed to model CVR benefits, and valid formulations are proposed that can be easily incorporated within the three-phase OPF model. Next, we develop valid linear and nonlinear approximations for the three-phase power flow equations. Based on the proposed linear and nonlinear power flow approximations, a bi-level framework is proposed for CVR. Level-1 solves MILP to obtain set points for legacy device and smart inverters using the linear OPF model. Level-2 solves a NLP (with linear objective and quadratic constraints) based on nonlinear OPF to further optimize the smart inverter parameters and result in a feasible power flow solution. Note that although energy savings are reported higher for meshed networks [24], a majority of distribution feeders in the United States are operated in radial topology. Therefore, this paper focuses on optimizing the operation of radially operated feeders. The specific contributions of this paper are detailed below.

- *Models for Voltage-dependent Loads and Voltage Control Devices:* Mathematical models for voltage-dependent loads and grid's voltage control devices including capacitor banks, voltage regulators and smart inverters are proposed. For loads, a novel CVR-based load model is proposed that approximates the ZIP load model. The proposed models can be easily absorbed into both levels of optimization problems without changing the types of equations.
- *Linear and Nonlinear Models for Three-phase Power Flow:* We develop valid linear and nonlinear approximations for three-phase unbalanced power flow model. The linear approximation is inspired by distflow equations but formulated for a three-phase unbalanced system. The nonlinear power flow is a new formulation and obtained by approximating the nonlinearities associated with the mutual coupling between the phases. Compared to the standard three-phase power flow formulations, the proposed model results in a reduced number of variables and introduces only nonlinearity of the nature of quadratic equality constraints.
- *Scalable Model for Coordinated Control of Legacy and New Voltage Control Devices for CVR:* The optimization problem for coordinated control of both legacy and new devices for a three-phase distribution feeder is a hard MINLP problem. To reduce complexity and enable scalability, we propose a bi-level approach by decomposing the MINLP into a MILP and a NLP. The scalability is demonstrated using IEEE 123-bus feeder (with 267 single-phase nodes) and 329-bus feeder (with 860 single-phase nodes). The proposed model solves 123-bus feeder within 4-mins and 329-bus feeder (after reduction) within 9-mins.
- *Validation using Multiple Test Feeders:* The proposed approach and all approximation steps are thoroughly validated against OpenDSS. First, the proposed three-phase

approximate power flow models are validated using IEEE 13-bus, IEEE 123-bus and 329-bus PNNL taxonomy feeders. Next, the accuracy of the proposed CVR-based load model is thoroughly validated against equivalent ZIP load models. Finally, the results for OPF are validated using OpenDSS.

The rest of the paper is organized as follows. Section II presents the proposed approximate models three-phase power flow. Section III details mathematical models for distribution system equipment. Section IV presents the proposed bi-level VVO approach followed by results in Section V and conclusion in Section VI.

II. Three-Phase Unbalanced Electric Power Distribution System

This section introduces the mathematical formulation for three-phase power flow based on branch-flow equations. Valid approximations are proposed to reduce the original formulation into a linear and an equivalent quadratic formulation.

A. Three-Phase Power Flow Using Branch Flow Model

Let, there be directed graph $\mathcal{G} = (\mathcal{N}, \mathcal{E})$ where $\mathcal{N}$ denotes set of buses and $\mathcal{E}$ denotes set of lines. Each line connects ordered pair of buses (i, j) between two adjacent nodes i and j. Let, $\{a, b, c\}$ denotes the three phases of the system and Φ_i denotes set of phases on bus i. For each bus $i \in \mathcal{N}$, let, phase p complex voltage is given by V_i^p and phase p complex power demand is $s_{L,i}^p$. Let, $V_i := [V_i^p]_{p\in\Phi_i}$ and $s_{L,i} := [s_{L,i}^p]_{p\in\Phi_i}$. For each line, let, p phase current be I_{ij}^p and define, $I_{ij} := [I_{ij}^p]_{p\in\Phi_i}$. Let, z_{ij} be the phase impedance matrix.

$$v_j = v_i - (S_{ij} z_{ij}^H + z_{ij} S_{ij}^H) + z_{ij} l_{ij} z_{ij}^H \quad (1)$$

$$\text{diag}(S_{ij} - z_{ij} l_{ij}) = \sum_{k:j\to k} \text{diag}(S_{jk}) + s_{L,j} \quad (2)$$

$$\begin{bmatrix} v_i & S_{ij} \\ S_{ij}^H & l_{ij} \end{bmatrix} = \begin{bmatrix} V_i \\ I_{ij} \end{bmatrix} \begin{bmatrix} V_i \\ I_{ij} \end{bmatrix}^H \quad (3)$$

$$\begin{bmatrix} v_i & S_{ij} \\ S_{ij}^H & l_{ij} \end{bmatrix} : -\text{Rank-1 PSD Matrix.} \quad (4)$$

A three-phase power flow formulation for a radial system based on branch flow relationship is given in [22] and detailed in (1)–(4). Here, (1) represents voltage drop equation, (2) corresponds to power balance equation, (3) are variable definitions for power flow quantities, and (4) is a Rank-1 constraint that makes the associated optimization problem non-convex. In the literature, methods are proposed to obtain a relaxed convex problem [25], [26], however, it is difficult to obtain a feasible solution from relaxed problem for a three-phase system [23]. Moreover, it is difficult to extend the power flow model detailed in (1)–(4) for voltage-dependent loads and system's legacy control devices. A new three-phase power flow model for OPF problem is called for that can easily incorporate system's critical components while not significantly increasing the inherent nonlinearity.

B. Approximate Three-Phase Power Flow Equations

In this section, we present valid linear and nonlinear power flow equations by approximating (1)–(4). Fundamentally, there are two reasons for nonlinearity in power flow equations: nonlinear relationship between power, voltage, and currents, and mutual coupling in a three-phase system. In the proposed formulation, the nonlinearity resulting from mutual coupling between the three phases is approximated. A phase-decoupled formulation by decoupling the branch power flow and voltage equations on a per-phase basis is obtained. The resulting three-phase power flow model characterizes the power flow equations using a fewer number of variables.

Define: $v_i^p = (V_i^p)^2$ where, $p \in \Phi_i$, $l_{ij}^{pq} = (|I_{ij}^p| \times |I_{ij}^q|)$ where, $(pq) \in \Phi_{ij}$, $\delta_{ij}^{pq} = \delta_{ij}^p - \delta_{ij}^q$, $S_{ij}^{pq} = P_{ij}^{pq} + jQ_{ij}^{pq}$, where, $(pq) \in \Phi_{ij}$, and $z_{i,j}^{pq} = r_{ij}^{pq} + jx_{ij}^{pq}$, where, $(pq) \in \Phi_{ij}$. Note that, $(l_{ij}^{pq})^2 = l_{ij}^{pp} \times l_{ij}^{qq}$ and δ_{ij}^{pq} is angle difference between branch currents I_{ij}^p and I_{ij}^q.

1) Assumption 1 - Approximating Phase Voltages: The phase voltages are assumed to exactly 120° degree apart. Moreover, it is assumed that the degree of unbalance in voltage magnitude is not large. Both conditions are valid for a distribution system as specified by the ANSI limits for bus voltages and phase unbalance [3].

$$\frac{V_i^a}{V_i^b} \simeq \frac{V_i^b}{V_i^c} \simeq \frac{V_i^c}{V_i^a} = e^{j*2\pi/3} = a^2 \quad (5)$$

Further note that

$$S_{ij}^{pq} = V_i^p \times I_{ij}^q \text{ and } S_{ij}^{qq} = V_i^q \times I_{ij}^q \quad (6)$$

Using (5) and (6), we express S_{ij}^{pq} as a function of S_{ij}^{qq} i.e. $S_{ij}^{pq} = \frac{V_i^p}{V_i^q} \times S_{ij}^{qq}$, where, $\frac{V_i^p}{V_i^q}$ is a constant (5). The off-diagonal elements of S_{ij} are approximated using diagonal terms which help reduce the number of power flow variables.

Note that the above conditions do not imply that a single-phase power flow will be sufficient to represent a distribution system. First, an equivalent single-phase model cannot represent two-phase or single-phase lines and loads. Second, it is imperative to solve for an unbalanced power flow even though the degree of voltage unbalance is less.

2) Assumption 2 – Approximating Angle Difference between Phase Currents: On expanding (1) and (2), nonlinearities are introduced as trigonometric functions of angle difference between the phase currents on a given three or two-phase line. Let, for a given line (i, j), the phase currents for phases p and q be $I_{ij}^p = |I_{ij}^p| \angle \delta_{ij}^p$, and $I_{ij}^q = |I_{ij}^q| \angle \delta_{ij}^q$. Then the angle difference between the phase currents of a given bus i i.e. $\delta_{ij}^{pq} = \angle\delta_{ij}^p - \angle\delta_{ij}^q$. We observe terms corresponding to $\sin(\delta_{ij}^{pq})$ and $\cos(\delta_{ij}^{pq})$ in power flow expressions. These terms significantly increase the complexity of the OPF problem.

In the proposed formulation, the phase angle difference between branch currents are approximated and modeled as a constant variable. An approximate value of δ_{ij}^{pq} for branch (i, j) is calculated by solving an equivalent distribution power flow with system loads modeled as constant impedance loads. We assume δ_{ij}^{pq} to be constant and equal to the one obtained by solving

power flow with constant impedance load model. Note that the constant impedance load model is only used to approximate δ_{ij}^{pq}. This assumption does not limit the type of load that can be incorporated in the proposed OPF model; it can easily incorporate all load types including constant power and constant current loads, as detailed in Section IV.

3) Power Flow Equations: The power flow equations defined in (1)–(4) are expanded. Using the above approximations, we are able to redefine the power flow equations in (1)–(4) as a set of linear and non-linear equations shown in (7)–(11). Here, (7)–(9) are linear in v_i^p, l_{ij}^{pq}, and S_{ij}^{pq}. Note that the total number of variables in the proposed formulation are $15 \times (n-1)$, where n is the number of nodes; the original formulation (1)–(4) had a total of $36 \times (n-1)$ variables

$$P_{ij}^{pp} - \sum_{q \in \Phi_j} l_{ij}^{pq} \left(r_{ij}^{pq} \cos\left(\delta_{ij}^{pq}\right) - x_{ij}^{pq} \sin\left(\delta_{ij}^{pq}\right) \right) = \sum_{k:j \to k} P_{jk}^{pp} + p_{L,j}^{p} \tag{7}$$

$$Q_{ij}^{pp} - \sum_{q \in \Phi_j} l_{ij}^{pq} \left(x_{ij}^{pq} \cos\left(\delta_{ij}^{pq}\right) + r_{ij}^{pq} \sin\left(\delta_{ij}^{pq}\right) \right) = \sum_{k:j \to k} Q_{jk}^{pp} + q_{L,j}^{p} \tag{8}$$

$$v_j^p = v_i^p - \sum_{q \in \Phi_j} 2\mathbb{R}\mathrm{e}\left[S_{ij}^{pq} (z_{ij}^{pq})^*\right] + \sum_{q \in \Phi_j} z_{ij}^{pq} l_{ij}^{qq} + \sum_{q1,q2 \in \Phi_j, q1 \neq q2} 2\mathbb{R}\mathrm{e}\left[z_{ij}^{pq1} l_{ij}^{q1q2} \left(\angle(\delta_{ij}^{q1q2}) \right) (z_{ij}^{pq2})^* \right] \tag{9}$$

$$(P_{ij}^{pp})^2 + (Q_{ij}^{pp})^2 = v_i^p l_{ij}^{pp} \tag{10}$$

$$(l_{ij}^{pq})^2 = l_{ij}^{pp} l_{ij}^{qq} \tag{11}$$

- (7) is written for all $(i,j) \in \mathcal{E}$ and represents the equation for active power flow on branch (i,j) for phase $pp \in \Phi_{ij}$. Since $\cos\left(\delta_{ij}^{pq}\right)$and $\sin\left(\delta_{ij}^{pq}\right)$ are assumed to be constant, this equation is linear in P_{ij}^{pp}, P_{jk}^{pp}, and l_{ij}^{pq}.
- (8) is written for all $(i,j) \in \mathcal{E}$ and represents the equation for reactive power flow on branch (i,j) for phase $pp \in \Phi_{ij}$. Similar to (7), (8) is linear in Q_{ij}^{pp}, Q_{jk}^{pp}, l_{ij}^{pq}.
- (9) represents the equation for voltage drop between the two nodes of branch (i,j) corresponding to phase p. The equation is also linear in v_i^p, v_j^p, and l_{ij}^{pq}.
- (10) relates per phase complex power flow in branch (i,j) to phase voltage and phase currents. This is a non-linear quadratic equality constraint.
- (11) simply relates current variables previously defined, i.e. $l_{ij}^{pq} = (|I_{ij}^p| \times |I_{ij}^q|), pq \in \Phi_{ij}$.

C. Linear Three-Phase AC Power Flow Approximation

The linear approximation assumes the branch power loss are relatively smaller as compared to the branch power flow [22]. The impact of power loss on active and reactive power branch flow equations and on voltage drop equations is ignored. After approximating (7)–(11), we obtain linearized AC branch flow equations as shown in (12)–(13). Here (12) corresponds to linearized active and reactive power flow and (13) corresponds to voltage drop equations

$$P_{ij}^{pp} = \sum_{k:j \to k} P_{jk}^{pp} + p_{L,j}^{p} \text{ and } Q_{ij}^{pp} = \sum_{k:j \to k} Q_{jk}^{pp} + q_{L,j}^{p} \tag{12}$$

$$v_j^p = v_i^p - \sum_{q \in \Phi_j} 2\mathbb{R}\mathrm{e}\left[S_{ij}^{pq} (z_{ij}^{pq})^*\right] \forall j \in Y_i. \tag{13}$$

The AC linearized power flow is significantly accurate in representing bus voltages. The linearized AC power flow, although does not include the impact of power loss on voltage drop, it does incorporate the impact of power flow due to load. Since power losses are significantly small as compared to the branch flow due to load demand, the obtained feeder voltages are good approximation of the actual feeder voltages [22].

III. Distribution System Equipment Models

This section details the models for capacitor banks, voltage regulators, smart inverters and voltage-dependent customer loads. The approximate power flow equations developed in Section II are a function of $v_i^p = |V_i^p|^2$. The equipment models are, therefore, parameterized based on respective control variables and the v_i^p. A new CVR based load model is developed to represent the power demand as a function of v_i^p. The ZIP coefficients for the load are used to obtain equivalent CVR coefficients. Note that the equipment and load models proposed in this section are specifically designed so that they can be easily absorbed within the approximate power flow equations defined in (7)–(13) without changing their type.

A. Voltage Regulator

A 32-step voltage regulator with a voltage regulation range of $\pm 10\%$ is assumed. The series and shunt impedance of the voltage regulator are ignored as these have very small value [27]. Let, a^p be the turn ratio for the voltage regulator connected to phase p of line (i,j). Then a^p can take values between 0.9 to 1.1 with each step resulting in a change of 0.00625 pu. An additional node i' is introduced to model the current equations. The control for regulator is defined using binary variables. Let, for $u_{tap,i}^p \in \{0,1\}$ be a binary variable defined for each regulator step position i.e. $i \in (1,2,\ldots,32)$. Also define a vector $b_i \in \{0.9, 0.90625, \ldots, 1.1\}$. Then V_i^p, V_j^p, $I_{ii'}^p$, and $I_{i'j}^p$ where $p \in \Phi_i \cap \Phi_j$ are given as follows:

$$V_j^p = V_{i'}^p = a^p V_i^p \text{ and } I_{ii'}^p = a^p I_{i'j}^p \tag{14}$$

where, $a^p = \sum_{i=1}^{32} b_i u_{tap,i}^p$ and $\sum_{i=1}^{32} u_{tap,i}^p = 1$.

In order to express (14) as a function of $v_i^p = (V_i^p)^2$, $v_j^p = (V_j^p)^2$, $l_{ii'}^{pp} = (I_{ii'}^p)^2$, and $l_{i'j}^{pp} = (I_{i'j}^p)^2$ we take square of (14) and define $a_p^2 = A_p$ and $b_i^2 = B_i$. Further realizing that $(u_{tap,i}^p)^2 = u_{tap,i}^p$, (14) can be reformulated as (15).

$$v_j^p = A^p \times v_i^p \text{ and } l_{ii'}^{pp} = A^p l_{i'j}^{pp} \tag{15}$$

B. Capacitor Banks

The per-phase model for capacitor banks is developed. The reactive power generated by capacitor bank, $q^p_{cap,i}$, is defined as a function of binary control variable $u^p_{cap,i} \in \{0,1\}$ indicating the status (On/Off) of the capacitor bank, its rated per-phase reactive power $q^{rated,p}_{cap,i}$, and the square of the bus voltage at bus i for phase p, v^p_i.

$$q^p_{cap,i} = u^p_{cap,i} q^{rated,p}_{cap,i} v^p_i. \tag{16}$$

The capacitor bank model is assumed to be voltage dependent and provides reactive power as a function of v^p_i when connected, i.e. $u_{cap,i} = 1$. For a three-phase capacitor bank, a common control variable, $u^p_{cap,i}$, is defined for each phase.

C. Distributed Generation With Smart Inverters

A per-phase model for reactive power support from smart inverter connected to DGs is developed. The DGs are modeled as negative loads with a known active power generation equal to the forecasted value. The reactive power support from DG depend upon the rating of the smart inverter. Let, the rated per-phase apparent power capacity for smart inverter connected to i^{th} DG be $s^{rated,p}_{DG,i}$ and the forecasted active power generation be $p^p_{DG,i}$. The available reactive power, $q^p_{DG,i}$ from the smart inverter is given by (17) which is a box constraint

$$-\sqrt{(s^{rated,p}_{DG,i})^2 - (p^p_{DG,i})^2} \le q^p_{DG,i} \le \sqrt{(s^{rated,p}_{DG,i})^2 - (p^p_{DG,i})^2}. \tag{17}$$

D. Voltage-Dependent Model for Customer Loads

The most widely acceptable load model is the ZIP model which is a combination of constant impedance (Z), constant current (I) and constant power (P)) characteristics of the load [28]. The mathematical representation of the ZIP model for the load connected at phase p of bus i is given by (18)–(19)

$$p^p_{L,i} = p^p_{i,0}\left[k_{p,1}\left(\frac{V^p_i}{V_0}\right)^2 + k_{p,2}\left(\frac{V^p_i}{V_0}\right) + k_{p,3}\right] \tag{18}$$

$$q^p_{L,i} = q^p_{i,0}\left[k_{q,1}\left(\frac{V^p_i}{V_0}\right)^2 + k_{q,2}\left(\frac{V^p_i}{V_0}\right) + k_{q,3}\right] \tag{19}$$

where, $k_{p,1} + k_{p,2} + k_{p,3} = 1$, $k_{q,1} + k_{q,2} + k_{q,3} = 1$, $p^p_{i,0}$ and $q^p_{i,0}$ are per-phase load consumption at nominal voltage, V_0.

The ZIP load model represented in (18)–(19) are a function of both V^p_i and $v^p_i = (V^p_i)^2$. Including (18) and (19) to OPF formulation will make (7), (8), (13), and (14), earlier linear in v^p_i, nonlinear. Here we develop an equivalent load model for voltage-dependent loads using the definition of CVR factor. Next, an equivalence between ZIP parameters and proposed CVR factors is obtained.

CVR factor is defined as the ratio of percentage reduction in active or reactive power to the percentage reduction in bus voltage. Let CVR factor for active and reactive power reduction be CVR_p, and CVR_q, respectively defined in (25).

$$CVR_p = \frac{dp^p_{L,i}}{p^p_{i,0}}\frac{V_0}{dV^p_i} \text{ and } CVR_q = \frac{dq^p_{L,i}}{q^p_{i,0}}\frac{V_0}{dV^p_i} \tag{20}$$

where, $p^p_{L,i} = p^p_{i,0} + dp^p_i$ and $q^p_{L,i} = q^p_{i,0} + dq^p_i$. Furthermore, $v^p_i = (V^p_i)^2$. Therefore, $dv^p_i = 2V^p_i dV^p_i$. Assuming $V^p_i \approx V_0$ and $dv^p_i = v^p_i - (V_0)^2$, we obtain:

$$p^p_{L,i} = p^p_{i,0} + CVR_p \frac{p^p_{i,0}}{2}\left(\frac{v^p_i}{V_0^2} - 1\right) \tag{21}$$

$$q^p_{L,i} = q^p_{i,0} + CVR_q \frac{q^p_{i,0}}{2}\left(\frac{v^p_i}{V_0^2} - 1\right) \tag{22}$$

Note that the CVR based load model detailed in (21) and (22) is linear in v^p_i, thus can be easily included in approximate power flow equations (7)–(13). The CVR factors, CVR_p and CVR_q are estimated from the ZIP coefficients of the load. On differentiating the ZIP model detailed in (18) and (19) and assuming $V_0 = 1$ p.u., we obtain:

$$\frac{dp^p_{L,i}}{dV^p_i} = p^p_{i,0}\left(2k_{p,1}V^p_i + k_{p,2}\right) \tag{23}$$

$$\frac{dq^p_{L,i}}{dV^p_i} = q^p_{i,0}\left(2k_{q,1}V^p_i + k_{q,2}\right) \tag{24}$$

Using (20), (23), (24) and assuming $V^p_i \approx V_0$, we obtain (25). Using (25), the CVR factors for customer loads can be obtained from the ZIP coefficients.

$$CVR_p = 2k_{p,1} + k_{p,2} \text{ and } CVR_q = 2k_{q,1} + k_{q,2} \tag{25}$$

IV. Proposed Bi-level Volt-VAR Optimization

The primary function of VVO is to use voltage control to 1) reduce energy consumption, 2) reduce system losses, and 3) regulate feeder voltages. The problem of coordinating the control of system's legacy devices and smart inverters results in an MINLP problem. To reduce complexity and ensure scalability, a bi-level approach is proposed.

1) Level 1: Develops a 15-min schedule for legacy devices and smart inverter reactive power demand set-points with the objective of minimizing the active power consumption for the feeder based on an MILP formulation.
2) Level 2: Develops revised 15-min schedule for smart inverter controls using a NLP formulation to achieve feasible three-phase power flow solutions. Level-2 uses the nonlinear power flow formulation proposed in Section II-C and obtains revised set points for smart inverter control that ensure feasible power flow solutions.

A. Level 1 - MILP Formulation for Coordinated Control

The objective of this stage is to minimize the power consumption for the feeder by controlling voltage regulators, capacitor banks, and smart inverters while ensuring that the voltage limits are satisfied. The control of legacy devices introduces integer variables into the optimization problem. A linear three-phase AC power flow is used and resulting problem is an MILP

formulation as detailed in (26)–(37). The objective is to minimize the sum of three-phase active power flowing out of the substation bus at time t (26). Here, $s \in \mathcal{N}$ denotes the substation bus. Since, the distribution feeder is radial, the substation power equals net feeder power demand.

Variables:
$u^p_{tap,i}(t)$, $u^p_{cap,i}(t)$, $q^p_{DG,i}(t)$, $v^p_i(t)$, $P^{pp}_{ij}(t)$, $Q^{pp}_{ij}(t)$, $S^{pq}_{ij}(t)$

$$\text{Minimize:} \sum_{p\in\Phi_s, j:s\to j} P^p_{sj}(t) \tag{26}$$

Subject to:

$$P^{pp}_{ij}(t) = \sum_{k:j\to k} P^{pp}_{jk}(t) + p^p_{L,j}(t) - p^p_{DG,i}(t) \forall i \in \mathcal{N} \tag{27}$$

$$Q^{pp}_{ij}(t) = \sum_{k:j\to k} Q^{pp}_{jk}(t) + q^p_{L,j}(t) - q^p_{DG,i}(t) - q^p_{C,i} \forall i \in \mathcal{N} \tag{28}$$

$$v^p_j(t) = v^p_i(t) - \sum_{q\in\Phi_j} 2\mathbb{R}\mathrm{e}\left[S^{pq}_{ij}(t)(z^{pq}_{ij})^*\right] \forall j \in Y_i \tag{29}$$

$$p^p_{L,i}(t) = p^p_{i,0}(t) + CVR_p(t)\frac{p^p_{i,0}(t)}{2}(v^p_i(t) - 1) \forall i \in \mathcal{N}_{\mathcal{L}} \tag{30}$$

$$q^p_{L,i}(t) = q^p_{i,0}(t) + CVR_q(t)\frac{q^p_{i,0}(t)}{2}(v^p_i(t) - 1) \forall i \in \mathcal{N}_{\mathcal{L}} \tag{31}$$

$$v^p_j(t) = A^p_i(t) v^p_i(t) \forall (i,j) \in \mathcal{E}_{\mathcal{T}} \tag{32}$$

$$A^p_i(t) = \sum_{i=1}^{32} B_i u^p_{tap,i}(t), \sum_{i=1}^{32} u^p_{tap,i}(t) = 1 \forall (i,j) \in \mathcal{E}_{\mathcal{T}} \tag{33}$$

$$q^p_{C,i}(t) = u^p_{cap,i}(t) q^{rated,p}_{cap,i} v^p_i(t) \forall (i) \in \mathcal{N}_{\mathcal{C}} \tag{34}$$

$$q^p_{DG,i}(t) \le \sqrt{(s^{rated,p}_{DG,i})^2 - (p^p_{DG,i})^2(t)} \forall (i) \in \mathcal{N}_{\mathcal{DG}} \tag{35}$$

$$q^p_{DG,i}(t) \ge -\sqrt{(s^{rated,p}_{DG,i})^2 - (p^p_{DG,i})(t)^2} \forall (i) \in \mathcal{N}_{\mathcal{DG}} \tag{36}$$

$$(V_{\min})^2 \le v^p_i(t) \le (V_{\max})^2 \forall i \in \mathcal{N} \tag{37}$$

- Constraints (27)–(29) are linear AC power flow constraints.
- Constraints (30)–(31) define CVR based load model.
- Constraints (32)–(33) define regulator control equations.
- Constraint (34) defines equations for capacitor control.
- Constraints (35)–(36) define control equations for reactive power dispatch at time t from smart inverters.
- Constraints (37) defines operating limits for feeder voltages.

B. Level 2 – NLP Problem for Smart Inverter Control

Level-1 uses a linear three-phase power flow model that approximates the losses. The solutions although feasible for linear power flow formulation, may violate the critical operating constraints of the feeder. The objective of this stage is to adjust the set-points of smart inverter control variables in order to obtain an optimal and feasible three-phase nonlinear power flow solution. The discrete control variables, $u^p_{tap,i}(t)$, $u^p_{cap,i}(t)$, are assumed to be fixed as obtained in Level-1. The optimal control set points for reactive power dispatch from smart inverters are obtained by solving the NLP problem (with linear objective and quadratic constraints) defined in (38)–(50).

Variables: $q^p_{DG,i}(t)$, $v^p_i(t)$, $P^{pp}_{ij}(t)$, $Q^{pp}_{ij}(t)$, $S^{pq}_{ij}(t)$, $l^{pq}_{ij}(t)$

$$\text{Minimize:} \sum_{p\in\Phi_s, j:s\to j} P^p_{sj}(t) \tag{38}$$

Subject to:

$$P^{pp}_{ij}(t) - \sum_{q\in\Phi_j} l^{pq}_{ij}(t)\left(r^{pq}_{ij}\cos(\delta^{pq}_{ij}(t)) - x^{pq}_{ij}\sin(\delta^{pq}_{ij}(t))\right) = \sum_{k:j\to k} P^{pp}_{jk}(t) + p^p_{L,j}(t) - p^p_{DG,i}(t) \forall i \in \mathcal{N} \tag{39}$$

$$Q^{pp}_{ij}(t) - \sum_{q\in\Phi_j} l^{pq}_{ij}(t)\left(x^{pq}_{ij}\cos(\delta^{pq}_{ij}(t)) + r^{pq}_{ij}\sin(\delta^{pq}_{ij}(t))\right) = \sum_{k:j\to k} Q^{pp}_{jk}(t) - q^p_{DG,i}(t) - q^p_{C,i}(t) \forall i \in \mathcal{N} \tag{40}$$

$$v^p_j(t) = v^p_i(t) - \sum_{q\in\Phi_j} 2\mathbb{R}\mathrm{e}\left[S^{pq}_{ij}(t)(z^{pq}_{ij})^*\right] + \sum_{q\in\Phi_j} z^{pq}_{ij} l^{qq}_{ij}(t) + \sum_{q1,q2\in\Phi_j, q1\ne q2} 2\mathbb{R}\mathrm{e}\left[z^{pq1}_{ij} l^{q1q2}_{ij}(t)\left(\angle(\delta^{q1q2}_{ij}(t))\right)(z^{pq2}_{ij})^*\right] \tag{41}$$

$$(P^{pp}_{ij}(t))^2 + (Q^{pp}_{ij}(t))^2 = v^p_i(t) l^{pp}_{ij}(t) \forall (i,j) \in \mathcal{E} \tag{42}$$

$$(l^{pq}_{ij}(t))^2 = l^{pp}_{ij}(t) l^{qq}_{ij}(t) \forall (i,j) \in \mathcal{E} \tag{43}$$

$$p^p_{L,i}(t) = p^p_{i,0}(t) + CVR_p(t)\frac{p^p_{i,0}(t)}{2}(v^p_i(t) - 1) \forall i \in \mathcal{N}_{\mathcal{L}} \tag{44}$$

$$q^p_{L,i}(t) = q^p_{i,0}(t) + CVR_q(t)\frac{q^p_{i,0}(t)}{2}(v^p_i(t) - 1) \forall i \in \mathcal{N}_{\mathcal{L}} \tag{45}$$

$$v^p_j(t) = A^p_i(t) v^p_i(t), A^p_i(t) = \sum_{i=1}^{32} B_i u^p_{tap,i}(t) \forall (i,j) \in \mathcal{E}_{\mathcal{T}} \tag{46}$$

$$q^p_{C,i}(t) = u^p_{cap,i}(t) q^{rated,p}_{cap,i} v^p_i(t) \forall (i) \in \mathcal{N}_{\mathcal{C}} \tag{47}$$

$$q^p_{DG,i}(t) \le \sqrt{(s^{rated,p}_{DG,i})^2 - (p^p_{DG,i})^2(t)} \forall (i) \in \mathcal{N}_{\mathcal{DG}} \tag{48}$$

$$q^p_{DG,i}(t) \ge -\sqrt{(s^{rated,p}_{DG,i})^2 - (p^p_{DG,i})(t)^2} \forall (i) \in \mathcal{N}_{\mathcal{DG}} \tag{49}$$

$$(V_{min})^2 \le v^p_i(t) \le (V_{max})^2 \forall i \in \mathcal{N} \tag{50}$$

- Constraints (39)–(43) are approximate nonlinear AC power flow equations defined at time t.
- Constraints (44)–(45) define CVR based load model.
- Constraints (46) define regulator control equations. Note that $u^p_{tap,i}$ is known from Level-1 solution.

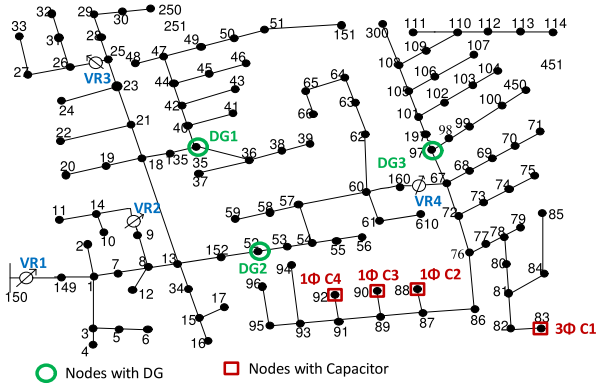

Fig. 1. IEEE 123-bus distribution test feeder.

- Constraint (47) defines control equations for capacitor banks at time t. Note that $u^{p}_{cap,i}$ is known from Level-1 solution.
- Constraints (48)–(49) define control equations for reactive power dispatch at time t from smart inverters.
- Constraints (50) defines operating limits for feeder voltages.

V. Results and Discussion

The proposed VVO approach is validated using following three test feeders: IEEE 13-bus, IEEE 123-bus [29], and PNNL 329-bus taxonomy feeder [30]. First, the proposed linear and nonlinear approximate power flow formulations are validated against the actual power flow solutions obtained using OpenDSS. Next, the proposed voltage-dependent load models are validated against equivalent ZIP load models. Finally, we demonstrate the proposed VVO approach using the aforementioned three test feeders. All simulations are done on MATLAB platform. Level-1 problem, modeled as MILP, is solved using CPLEX 12.7 and Level-2 problem, modeled as NLP, is solved using fmincon function in MATLAB optimization toolbox. A computer with core i7 3.41 GHz processor with 16 GB of RAM has been used for the simulations. The results obtained from MATLAB are validated against OpenDSS.

IEEE-13 bus is a small highly loaded unbalanced distribution feeder operating at 4.16 kV making it a good candidate for testing VVO applications. This test feeder includes a three-phase and a single-phase capacitor bank and a voltage regulator at the substation. A PV with smart inverter of 575 kVA rated capacity is installed at node 671. IEEE-123 bus feeder also presents unbalanced loading conditions and several single-phase lines and loads with voltage drop problems making it a good candidate for demonstration of VVO application. There are four voltage regulators and four capacitor banks deployed along the feeder as shown in Fig. 1. The feeder is modified to include three DGs of capacity 345 kVA, 345 kVA, and 690 kVA at nodes 35, 52, and 97 respectively (see Fig. 1). The 329-bus feeder is used to demonstrate the scalability of the proposed approach. Notice that 329-bus feeder includes 329 physical nodes and a total of 860 single-phase nodes. Compared to the state-of-art, this is a significantly large test system to demonstrate the coordinated control of all voltage control devices. The feeder includes one voltage regulator, one 600 kVAr three-phase capacitor bank, three 100 kVAr single-phase capacitor banks, and three DGs of capacity 23 kVA, 57.5 kVA and 115 kVA (see Fig. 2).

Customer loads are assumed to have a CVR factor of 0.6 for active power and 3 for reactive power [2]. Note that the CVR values are arbitrary and can be easily adjusted based on the parameters for ZIP model of the load, if available, as detailed in Section III-D. To demonstrate the applicability of the proposed approach for different load mix, additional cases are simulated using a combination of residential and small and large commercial loads. The daily load and generation profiles are simulated in 15-min interval and are based on example profiles provided in OpenDSS (see Fig. 3).

A. Verification of Approximate Power Flow Formulations

This section validates the proposed approximate power flow models. The results obtained from the proposed linear and nonlinear power flow models are compared with the power flow solution obtained using OpenDSS (see Table I). The largest errors in active and reactive power flow and bus voltages are reported for the three test feeders in Table I for different loading conditions. Note that the three-phase linear power model is sufficiently accurate in modeling power flow equations for an unbalanced system. Since, the losses are ignored in flow equations (equation (12)), the linear model incurs higher error in flow quantities (P_{flow}, and Q_{flow}). However, since the voltage drop due to flow quantities is included in linear model (equation (13)), the bus voltages are well approximated. Another key observation is an increase in error in Q_{flow} vs. P_{flow} for 123-bus and 329-bus feeders. The approximation errors in flow quantities using the linearized model depend upon relative values of line resistance and reactance. The line reactance is higher than the line resistance for these two feeders leading to more reactive power losses and hence a higher error in approximating Q_{flow} quantities using linearized model. The nonlinear power flow model includes losses in the formulation and, therefore, results in lesser error in both flow quantities and bus voltages. The maximum error in bus voltages during peak load using linear and nonlinear models are: 0.0096 pu and 0.0025 pu for the 13-bus, 0.0074 pu and 0.0016 pu for the 123-bus, and 0.002 and 0.0002 pu for 329-bus systems, respectively. Note that 329-bus feeder is relatively more balanced and, therefore, incurs less error in voltages as compared to the rest of the two feeders.

The proposed nonlinear power flow formulation is based on two approximations: 1) difference between phase angles of node voltage (θ_i^{pq}) is close to 120°, 2) difference between phase angles of branch currents (δ_{ij}^{pq}) is close to those obtained using a constant impedance load model. These approximations are validated in Table II. The table reports largest deviation between actual quantities obtained using OpenDSS vs. the approximated ones used in this paper. As it can be seen, the largest error is less than 2° for both voltage and current phase angle difference.

The proposed nonlinear power flow is verified at heavily unbalanced loading for IEEE 123 node and 329 node system. The unbalanced in the system is created by increasing the load for

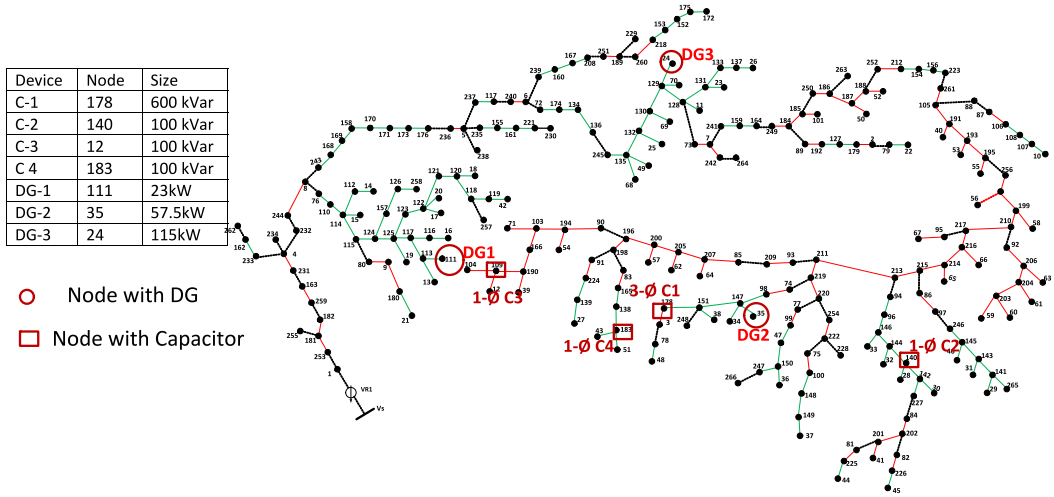

Fig. 2. PNNL 329-bus taxonomy distribution test feeder.

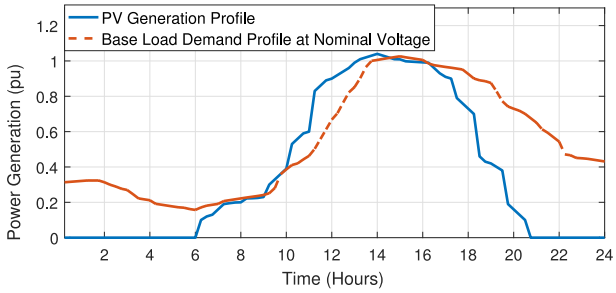

Fig. 3. Load demand and PV generation in 15-min interval.

TABLE I
COMPARISON OF APPROXIMATE LINEAR AND NONLINEAR POWER FLOW FORMULATIONS AGAINST OPENDSS SOLUTIONS

Largest Error in Linear Power Flow wrt. OpenDSS Solutions				
Test Feeder	% Loading	$P_{flow}(\%)$	$Q_{flow}(\%)$	V(pu.)
IEEE 13 Bus	75%	5.1287	4.938	0.0075
IEEE 13 Bus	100%	7.227	6.442	0.0096
IEEE 123 Bus	75%	5.248	9.502	0.0054
IEEE 123 Bus	100%	5.328	11.313	0.0074
PNNL 329 Bus	75%	1.16	6.9	0.001
PNNL 329 Bus	100%	1.55	9.51	0.002
Largest Error in Nonlinear Power Flow wrt. OpenDSS Solutions				
Test Feeder	% Loading	$P_{flow}(\%)$	$Q_{flow}(\%)$	V(pu.)
IEEE 13 Bus	75%	0.2414	1.668	0.0015
IEEE 13 Bus	100%	0.297	2.034	0.0025
IEEE 123 Bus	75%	0.505	2.58	0.0014
IEEE 123 Bus	100%	0.606	3.88	0.0016
PNNL 329 Bus	75%	0.3	2.2	0.0001
PNNL 329 Bus	100%	0.6	3.4	0.0002

one of the phase. The voltage unbalance defined in (51) according to IEEE definition, is used to quantify the effect of load unbalance created in the system.

$$V_{unbalance} = \frac{max.deviation}{|V_{avg}|} * 100. \qquad (51)$$

TABLE II
MAXIMUM ERROR IN APPROXIMATING PHASE ANGLE DIFFERENCES

Test Feeder	% Load	error in δ_{ij}^{pq}	error in θ_i^{pq}
IEEE 13 Bus	75%	1.8	1.8
IEEE 13 Bus	100%	2.1	2.2
IEEE 123 Bus	75%	0.8	0.9
IEEE 123 Bus	100%	1.13	1.3
PNNL 329 Bus	75%	0.5	0.55
PNNL 329 Bus	100%	0.9	1.05

TABLE III
COMPARISON OF APPROXIMATE NONLINEAR POWER FLOW FORMULATIONS AGAINST OPENDSS SOLUTIONS

Error in Nonlinear Power Flow wrt. OpenDSS during unbalanced loading				
Test Feeder	$V_{unbal}(\%)$	$P_{flow}(\%)$	$Q_{flow}(\%)$	V(pu.)
IEEE 123 Bus	3.2	0.61	3.88	0.0016
IEEE 123 Bus	5.7	0.68	3.94	0.004
PNNL 329 Bus	2.8	0.52	3.74	0.0007
PNNL 329 Bus	4.5	0.82	3.91	0.001

The IEEE-123 node system has the inherent apparent power unbalance of 23.2%, which creates a maximum voltage unbalance of 3.2%. Further, to produce more unbalance in the system the apparent power of phase A is increased which results in apparent power unbalance of 39.6%. Due to increased power unbalance the maximum voltage unbalance in the system is 5.7%. The maximum error in P_{flow}, Q_{flow} and voltage is shown in Table III for IEEE-123 node system for both the test case. It is known that the 329 bus system is a balanced system. Hence, to generate unbalance in the system the apparent power of phase B is increased which originates to apparent power unbalanced of 40.72% and 57.39%. The effect of unbalanced power results in voltage unbalanced of 2.8% and 4.5% respectively. The maximum error in P_{flow}, Q_{flow} and voltage with respect OpenDSS power flow results is shown in Table III. It is required to mention that the nonlinear power flow is solved at flat start. According to ANSI C84.1 electric system can have the maximum voltage

TABLE IV
ZIP COEFFICIENTS FOR DIFFERENT CLASS OF LOADS

Load Class	Z_p	I_p	P_p	Z_q	I_q	Q_q	CVR_p	CVR_q
Residential	0.96	-1.17	1.21	6.28	-10.16	4.88	0.75	2.4
Small Commercial	0.77	-0.84	1.07	8.09	-13.65	6.56	0.7	2.53
Large Commercial	0.4	-0.41	1.01	4.43	-7.99	4.56	0.39	0.87

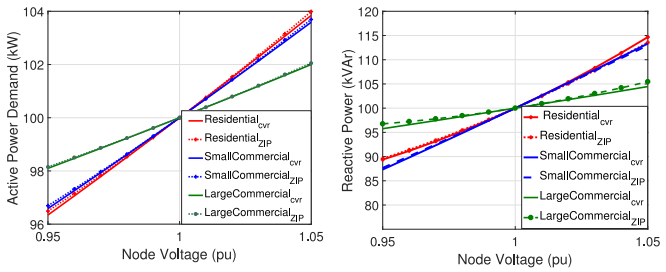

Fig. 4. Comparison of proposed load model with ZIP model. (a) Active power demand. (b) Reactive power demand.

unbalance of 3%. Hence, Table III uphold the proposed power flow can be used for the heavily unbalanced system.

B. Validation of Proposed CVR-Based Load Model

The proposed CVR-based voltage dependent load model derived in equations (21)–(22) is validated against equivalent ZIP load models detailed in equations (18)–(19). When accurately modeled, the CVR-based load model should require the same power demand as the equivalent ZIP load model for the acceptable range of operating voltages (0.95 pu–1.05 pu). Therefore, to validate the load models, the active and reactive power consumption for CVR-based load models are compared against the power consumption for ZIP load model for varying node voltages. ZIP models for residential, small commercial, and large commercial loads are used for validation. The ZIP coefficients for the different class of loads are obtained from [28] and converted to CVR-based load model using equation (25) (also see Table IV).

The simulation case is detailed here. For each load class, the base active $p_{i,0}$ and $q_{i,0}$ reactive power are taken as 100 kW and 100 kVAr, respectively. The voltage at the load point is varied from 0.95 to 1.05 pu. The active and reactive power demand for the two load models are shown in Fig. 4. It can be observed that for different load classes, the variation in power demand, both active and reactive, due to change in bus voltage are similar for both CVR-based load model and equivalent ZIP load model.

C. CVR Using Proposed VVO Approach

The proposed bi-level VVO approach is validated using IEEE test feeders. The optimal control set points are obtained for both legacy and smart inverter control devices for the entire day. The results demonstrate that the proposed formulation ensures that feeder operates closer to minimum voltage range while not violating the voltage limit constraints and therefore, is effective in achieving CVR objectives.

TABLE V
VOLT-VAR OPTIMIZATION RESULTS FOR IEEE 13-BUS FEEDER
($CVR_p = 0.6$ AND $CVR_q = 3$)

IEEE-13	Minimum Load			Maximum Load		
OPF solution from MATLAB						
Phase	A	B	C	A	B	C
Regulator Tap	-13	-13	-13	14	14	14
Cap1 Status	OFF	OFF	OFF	OFF	OFF	OFF
Cap2 Status	—	—	OFF	—	—	ON
DG1 q^p_{DG}(MVAR)	-0.04	-0.13	-0.03	-0.30	-0.45	0.12
Optimal substation power flow and voltages using MATLAB						
Load (MW)	0.143	0.132	0.091	0.866	0.622	0.685
Min. Voltage (pu)	0.955	0.956	0.955	0.95	0.955	0.95
Max. Voltage (pu)	0.97	0.97	0.97	1.03	1.03	1.03
Avg. Voltage (pu)	0.958	0.956	0.958	0.972	0.971	0.972
Validation of substation power flow and voltages using OpenDSS						
Load (MW)	0.144	0.135	0.095	0.87	0.625	0.69
Min. Voltage (pu)	0.955	0.955	0.955	0.95	0.953	0.95
Max. Voltage (pu)	0.97	0.97	0.97	1.03	1.03	1.03
Avg. Voltage (pu)	0.958	0.956	0.958	0.971	0.97	0.971

1) IEEE 13-Bus Test System: The control variables for this feeder include a 32-step three-phase voltage regulator, a three-phase capacitor bank (Cap1), a single-phase capacitor bank on Phase C (Cap2), and one three-phase DG with smart inverter control. The model is simulated in 15-min interval for 1 day. The results obtained for the day during minimum and maximum loading conditions are shown in Table IV. As it can be seen that the feeder is unbalanced with a largest difference of around 0.24 MW during peak load condition. Based on the table, with the increase in load, regulator tap position changes from -13 at minimum load condition to 14 at maximum load condition. The three-phase capacitor bank is OFF for both load conditions, while single-phase capacitor in ON during peak load condition. For each phase, DG is supplying reactive power in order to maintain the feeder voltages within the ANSI limits except for phase C during maximum load condition. This is because the single-phase capacitor is ON and supplies the required reactive power. It should also be noted that the absorbed power supplied by DG increases with the loading. The average feeder voltage seen at both maximum and minimum loading conditions are close to 0.96 pu. The proposed VVO approach is, therefore, successful in maintaining feeder voltages close to minimum voltage limit, thus help extract the CVR benefits.

The results obtained from the proposed approach are validated using OpenDSS. The optimal controls obtained from MATLAB for both maximum and minimum load conditions are implemented on 13-bus test feeder. The test feeder, with given statuses of voltage control devices, is solved using OpenDSS and substation power demand and minimum, maximum, and average node voltages are recorded (see Table V). It is observed that the system parameters obtained from MATLAB and OpenDSS closely match. This is expected given the accuracy of the proposed nonlinear power flow model.

The optimal power consumption as recorded at the substation transformer after implementing the proposed VVO strategy for the day is shown in Fig. 5. The total power demand is compared

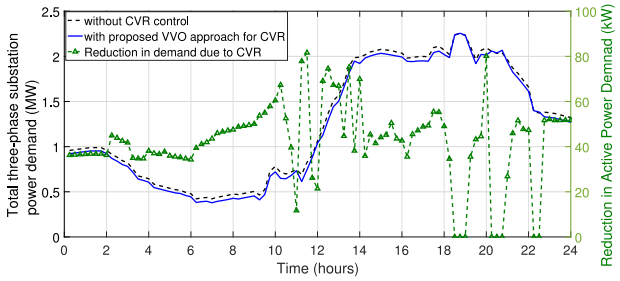

Fig. 5. IEEE-13 Bus CVR benefits observed using the proposed approach ($CVR_p = 0.6$ and $CVR_q = 3$).

TABLE VI
CVR FOR IEEE 13-BUS FEEDER

Load Composition	Minimum Load		Maximum Load	
	CVR	No CVR	CVR	No CVR
100% R	0.463	0.481	2.096	2.233
70% R, 30% SC	0.465	0.480	2.098	2.234
50% R, 30% SC, 20% LC	0.468	0.475	2.103	2.237

R-Residential, SC-Small Commercial, LC-Large Commercial

with the case when VVO is not enabled. For this case, the capacitors and voltage regulators work in autonomous control mode while DG is operating at unity power factor. Except for peak demand duration, the proposed approach results in a reduction in net power demand. The largest reductions are seen at low loading condition.

To further validate the proposed approach, we include additional test results with realistic load models for residential, commercial and large commercial loads. The ZIP coefficients details in Table IV are used to obtain CVR factors for each case with different load mix. The total load demand for minimum and maximum load conditions are reported in Table VI. It can be observed that the reduction in active power demand is lower for load mix with large commercial load as it shows less sensitivity to voltage.

Computational Complexity: On an average on a dual core i7 3.41 GHz processor with 16 GB of RAM, the Level-1 solutions are obtained in less than 5 sec and Level-2 solutions are obtained within 9 sec for the 13-bus system. The largest time taken for solving Level-2 problem is 14 sec.

2) IEEE 123-bus test system: Similarly, the proposed bi-level VVO approach is implemented using IEEE 123-node system for 1 day at 15-min interval. The results obtained from VVO for 123-node system are shown Table VII. The feeder is unbalanced with Phase B load being less than Phase A and C. The voltage regulator, Reg1, located at substation transformer (see Fig. 1), is at -13 tap for minimum load and -8 tap at maximum load. The voltage regulator, Reg4 is always at tap 0. Voltage regulators 2 and 3 are single and two-phase devices respectively and operate as optimization program instructs. Cap1 is a three-phase device and is OFF during minimum load and ON at maximum load condition and supplies required reactive power to maintain the voltage profile. Cap2, Cap3 and Cap4 are single phase devices and are ON/OFF depending upon the load demand.

TABLE VII
VOLT-VAR OPTIMIZATION RESULTS FOR IEEE 123-NODE FEEDER
($CVR_p = 0.6$ AND $CVR_q = 3$)

IEEE-123	Minimum Load			Maximum Load		
Phase	A	B	C	A	B	C
OPF solution from MATLAB						
Reg1 Tap	-13	-13	-13	-8	-8	-8
Reg2 Tap	0	—	—	-2	—	—
Reg3 Tap	1	—	1	7	—	2
Reg4 Tap	0	0	0	0	0	0
Cap1 Status	OFF	OFF	OFF	ON	ON	ON
Cap2 Status	OFF	—	—	ON	—	—
Cap3 Status	—	OFF	—	—	OFF	—
Cap4 Status	—	—	OFF	—	—	OFF
DG1 q^p_{DG}(MVAR)	-0.03	0.045	0.012	-0.028	0.03	0.04
DG2 q^p_{DG}(MVAR)	0.04	-0.03	0.03	-0.025	0.039	-0.01
DG3 q^p_{DG}(MVAR)	-0.08	-0.02	-0.08	-0.09	0.045	-0.09
Optimal substation power flow and voltages using MATLAB						
Load (MW)	0.20	0.13	0.18	0.99	0.78	1.02
Min. Voltage (pu)	0.955	0.955	0.955	0.951	0.953	0.951
Max. Voltage (pu)	0.965	0.965	0.965	0.995	0.995	0.995
Avg. Voltage (pu)	0.957	0.957	0.958	0.963	0.965	0.966
Validation of substation power flow and voltages using OpenDSS						
Load (MW)	0.205	0.134	0.183	1.00	0.79	1.024
Min. Voltage (pu)	0.954	0.954	0.954	0.95	0.95	0.95
Max. Voltage (pu)	0.965	0.965	0.965	0.995	0.995	0.995
Avg. Voltage (pu)	0.956	0.956	0.956	0.96	0.961	0.963

TABLE VIII
CVR FOR IEEE 123-BUS FEEDER

Load Composition	Minimum Load		Maximum Load	
	CVR	No CVR	CVR	No CVR
100% R	0.588	0.777	2.726	2.842
70% R, 30% SC	0.588	0.776	2.727	2.846
50% R, 30% SC, 20% LC	0.589	0.748	2.728	2.859

R-Residential, SC-Small Commercial, LC-Large Commercial

The DGs are located at three-phase nodes (see Fig. 1). Compared to minimum load condition, the reactive power demand or generation for DG1 and DG3 does not change significantly, except DG3. In contrast with minimum loading, DG3 is absorbing reactive power in Phase B during maximum load condition. Since Reg3 does not change the tap position, Phase B of DG3 adjusts the set points to account for the increase in load. Similarly, since there is no other VVC device between Reg1 and DG2, there is a drastic change in optimal DG behaviour between the two load conditions. The feeder voltage characteristics are also shown in Table VII. On an average the feeder operates close to minimum voltage limit, i.e. 0.96 pu, for both load conditions.

The bi-level VVO approach is validated against OpenDSS. The optimal status of capacitor banks switch, voltage regulator tap, and reactive power reference to the DGs, obtained from MATLAB, are implemented on OpenDSS model for the 123-bus system. The substation power demand and feeder voltage characteristics obtained using MATLAB are validated against OpenDSS (see Table VIII). The system parameters obtained from MATLAB closely match to those obtained from OpenDSS thus validating the VVO model.

Finally, the CVR benefits obtained using the proposed approach are reported. The total three-phase substation load

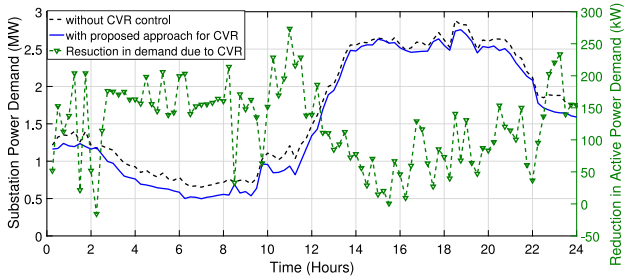

Fig. 6. IEEE-123 CVR benefits observed using the proposed approach ($CVR_p = 0.6$ and $CVR_q = 3$).

demand is compared to the case when VVO control is not enabled as shown in Fig. 6. On an average a reduction of around 150 kW is reported in net feeder active power demand. As expected the largest savings are reported during the minimum load condition.

The proposed approach is further validated using ZIP load models for residential, commercial and large commercial loads. The ZIP coefficients detailed in Table IV are used to obtain CVR factors for each case with different load mix. The total feeder load demand for the minimum and maximum load condition are reported in Table VIII.

Computational Complexity: On an average on a dual core i7 3.41 GHz processor with 16 GB of RAM, the Level-1 solutions are obtained in less than 5 sec for 123-bus system. For 123-bus, Level-1 solves 800 MILP equations with 1160 variables. On an average it takes 2-min to solve Level-2 problem for 123-bus system. The largest time taken for solving Level-2 problem for 123-bus system is 4 min. The Level-2 problem for 123-bus system solves 795 linear and 528 nonlinear equations (quadratic equalities) and with 1263 variables. The Level-1 and Level-2 solution times are within the 15-min control interval. Note that 123-bus test feeder represents a practical mid-size primary distribution circuit. The test feeder has 123 buses and a total of 267 single-phase nodes.

It should be noted that the Level-1 formulation scales well for larger feeders. This is because Level-1 solves an MILP that is relatively easier to solve even for a large set of constraints. The NLP problem in Level-2, however, is more difficult to scale for a large distribution system. In such cases, network reduction techniques are needed to represent the system with fewer equations [31]. In the following section, we demonstrate the scalability of the proposed approach using a 329-bus three-phase distribution feeder with the help of a simple network reduction technique.

3) 329-bus PNNL Taxonomy Feeder: The selected PNNL taxonomy feeder includes 329 buses, where, the number of nodes for phases A, B and C are 288, 298 and 274, respectively (total 860 single-phase nodes) (see Fig. 2). The proposed bi-level approach is implemented on 329-bus system. It is observed that Level-1 problem (MILP) takes on an average 20-sec. to solve, however, Level-2 problem (NLP) takes on an average 20-mins. Note that Level-2, for 329-bus system, solves for 4233 variables. In order to scale the Level-2 problem and to obtain a solution within 15-min interval, the 329-bus system is reduced using a simple network reduction technique. To reduce the network, we used the property of radial distribution feeders; the nodes that do not include branches, loads, or voltage control devices are combined using the equations for the series system for the corresponding branches. Using this method, the 329-bus system is reduced to a 184-bus system where, the number of nodes in phase A, B and C are 163, 171 and 156, respectively. After network reduction, the total number of variables for the Level-2 problem are reduced to 2415. Since network reduction is exact both models result in same power flow quantities. The Level-2 problem is implemented using 184-bus reduced network. The maximum computation time required to solve the Level-2 problem for the reduced network model is 9 mins.

TABLE IX
VOLT-VAR OPTIMIZATION RESULTS FOR 329-NODE FEEDER

IEEE-329	Minimum Load			Maximum Load		
Phase	A	B	C	A	B	C
OPF solution from MATLAB						
Reg1 Tap	-6	-6	-6	1	1	1
Cap1 Status	OFF	OFF	OFF	ON	ON	ON
Cap2 Status	OFF	—	—	OFF	—	—
Cap3 Status	—	OFF	—	—	OFF	—
Cap4 Status	—	—	OFF	—	—	OFF
DG1 q^p_{DG}(MVAR)	0.02	0.02	0.02	0.01	0.01	0.01
DG2 q^p_{DG}(MVAR)	-0.06	-0.06	-0.06	-0.03	-0.03	-0.03
DG3 q^p_{DG}(MVAR)	-0.11	-0.11	-0.08	0.055	0.035	0.022
Optimal substation power flow and voltages using MATLAB						
Load (MW)	0.444	0.459	0.434	2.86	2.97	2.775
Min. Voltage (pu)	0.958	0.958	0.958	0.955	0.955	0.955
Max. Voltage (pu)	0.962	0.962	0.962	1.0063	1.0063	1.0063
Avg. Voltage (pu)	0.959	0.959	0.959	0.974	0.972	0.976
Validation of substation power flow and voltages using OpenDSS						
Load (MW)	0.445	0.462	0.438	2.87	2.98	2.79
Min. Voltage (pu)	0.958	0.958	0.958	0.954	0.953	0.954
Max. Voltage (pu)	0.962	0.962	0.962	1.0063	1.0063	1.0063
Avg. Voltage (pu)	0.959	0.959	0.959	0.971	0.97	0.973

The CVR results obtained for maximum and minimum load conditions are shown in Table IX. Note that the Level-1 problem is implemented using full 329-bus feeder and the Level-2 problem is implemented using reduced 184-bus feeder. As the load is closely balanced, the behavior of each phase is almost similar. The voltage regulator at the substation is at -6 tap for the minimum load and at 1 tap position for the maximum load condition. At minimum load, the three-phase as well as single-phase capacitor banks are OFF. However, at the maximum load condition, the three-phase capacitor is ON and single-phase capacitor banks are OFF. The reactive power support from DG1 is same for all phases for both maximum and minimum load conditions. The minimum voltage for all the phases is at 0.958 pu at minimum load condition and at 0.955 pu at maximum load. The average voltage along the feeder is 0.959 and 0.972 at minimum and maximum load conditions, respectively. The substation power demand and feeder voltage characteristics obtained using MATLAB are validated against OpenDSS (see Table IX). The system parameters obtained from MATLAB closely match to those obtained from OpenDSS, validating the proposed VVO model.

The CVR benefits obtained using the proposed approach for 24-hour duration are reported in Fig. 7. The total three-phase substation load demand is compared to the case when VVO

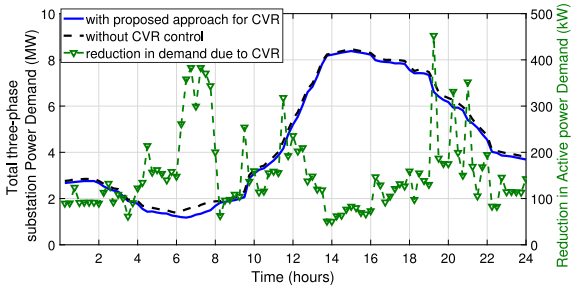

Fig. 7. 329-bus CVR benefits observed using the proposed approach ($CVR_p = 0.6$ and $CVR_q = 3$).

control is not enabled. On an average a reduction of around 200 kW is reported in the net feeder active power demand.

VI. Conclusion

This paper presents a VVO approach for CVR by coordinating the operation of distribution system's legacy voltage control devices and smart inverters. A bi-level VVO framework based on mathematical optimization techniques is proposed to efficiently handle the discrete and continuous control variables. The proposed approach solves OPF for a three-phase unbalanced electric power distribution system. The Level-1 solves a MILP problem to obtain control setpoints for both legacy devices and smart inverters using linear approximation for three-phase OPF. Next, Level-2 freezes the control for legacy devices and solves a NLP problem (with linear objective and quadratic constraints) to obtain a feasible and optimal solution by adjusting the setpoints for DG control using an approximate nonlinear OPF model. The approach is thoroughly validated using three test feeders, IEEE 13-bus, IEEE 123-bus, and PNNL 329-bus taxonomy feeders. The results demonstrate that: 1) the proposed power flow approximations are reasonably accurate, 2) the proposed approach successfully coordinates the operation of legacy and new devices for CVR benefits, and 3) both Level-1 and Level-2 solutions are computationally efficient for a realtime operation.

References

[1] K. P. Schneider, J. C. Fuller, F. K. Tuffner, and R. Singh, "Evaluation of conservation voltage reduction (CVR) on a national level," Pacific Northwest Nat. Laboratory, Richland, WA, USA, Tech. Rep. PNNL-19596, 2010.

[2] K. Forsten, "Green circuits: Distribution efficiency case studies," Elect. Power Res. Inst., Palo Alto, CA, USA, Tech. Rep. 1023518, 2011.

[3] *American National Standard For Electric Power Systems and Equipment-Voltage Ratings (60 Hertz)*, American National Standards Institute C84.1-2016, 2011.

[4] M. E. Baran and M.-Y. Hsu, "Volt/VAr control at distribution substations," *IEEE Trans. Power Syst.*, vol. 14, no. 1, pp. 312–318, Feb. 1999.

[5] T. T. Hashim, A. Mohamed, and H. Shareef, "A review on voltage control methods for active distribution networks," *Elect. Rev.*, vol. 88, pp. 304–312, 2012.

[6] H. V. Padullaparti, Q. Nguyen, and S. Santoso, "Advances in volt-var control approaches in utility distribution systems," in *Proc. IEEE Power Energy Soc. General Meeting*, Jul. 5, 2016, pp. 1–5.

[7] B. Green, "Grid Strategy 2011: Conservation voltage reduction and volt VAR optimization in the smart grid," Electr. Power Res. Inst., Palo Alto, CA, USA, Tech. Rep. 1024482, 2011.

[8] G. L. Barbose, "U.S. Renewables Portfolio Standards: 2017 Annual Status Report," Clean Energy Group, Montpelier, VT, USA, Tech. Rep. LBNL-2001031, 2017.

[9] A. Bokhari *et al.*, "Combined effect of CVR and DG penetration in the voltage profile of low-voltage secondary distribution networks," *IEEE Trans. Power Del.*, vol. 31, no. 1, pp. 286–293, Feb. 2016.

[10] M. Farivar, R. Neal, C. Clarke, and S. Low, "Optimal inverter VAR control in distribution systems with high PV penetration," in *Proc. IEEE Power Energy Soc. General Meeting*, Jul. 2012, pp. 1–7.

[11] H. Zhu and H. J. Liu, "Fast local voltage control under limited reactive power: Optimality and stability analysis," *IEEE Trans. Power Syst.*, vol. 31, no. 5, pp. 3794–3803, Sep. 2016.

[12] V. Kekatos, L. Zhang, G. B. Giannakis, and R. Baldick, "Fast localized voltage regulation in single-phase distribution grids," in *Proc. IEEE Int. Conf. Smart Grid Commun.*, Nov. 2015, pp. 725–730.

[13] E. DallAnese, S. V. Dhople, B. B. Johnson, and G. B. Giannakis, "Decentralized optimal dispatch of photovoltaic inverters in residential distribution systems," *IEEE Trans. Energy Convers.*, vol. 29, no. 4, pp. 957–967, Dec. 2014.

[14] X. Su, M. A. S. Masoum, and P. J. Wolfs, "Optimal PV inverter reactive power control and real power curtailment to improve performance of unbalanced four-wire LV distribution networks," *IEEE Trans. Sustain. Energy*, vol. 5, no. 3, pp. 967–977, Jul. 2014.

[15] H. Ahmadi, J. R. Mart, and H. W. Dommel, "A framework for volt-VAR optimization in distribution systems," *IEEE Trans. Smart Grid*, vol. 6, no. 3, pp. 1473–1483, May 2015.

[16] T. V. Dao, S. Chaitusaney, and H. T. N. Nguyen, "Linear least-squares method for conservation voltage reduction in distribution systems with photovoltaic inverters," *IEEE Trans. Smart Grid*, vol. 8, no. 3, pp. 1252–1263, May 2017.

[17] Z. Wang, J. Wang, B. Chen, M. M. Begovic, and Y. He, "MPC-based voltage/var optimization for distribution circuits with distributed generators and exponential load models," *IEEE Trans. Smart Grid*, vol. 5, no. 5, pp. 2412–2420, Sep. 2014.

[18] D. Ranamuka, A. P. Agalgaonkar, and K. M. Muttaqi, "Online voltage control in distribution systems with multiple voltage regulating devices," *IEEE Trans. Sustain. Energy*, vol. 5, no. 2, pp. 617–628, Apr. 2014.

[19] M. S. Hossan, B. Chowdhury, M. Arora, and C. Lim, "Effective CVR planning with smart DGs using MINLP," in *Proc. North Amer. Power Symp.*, Sep. 6 , 2017, pp. 1–6.

[20] F. Ding *et al.*, "Application of autonomous smart inverter volt-var function for voltage reduction energy savings and power quality in electric distribution systems," in *Proc. IEEE Power Energy Soc. Innovative Smart Grid Technol. Conf.*, Apr. 6, 2017, pp. 1–5.

[21] M. Liu, C. A. Canizares, and W. Huang, "Reactive power and voltage control in distribution systems with limited switching operations," *IEEE Trans. Power Syst.*, vol. 24, no. 2, pp. 889–899, May 2009.

[22] L. Gan and S. H. Low, "Convex relaxations and linear approximation for optimal power flow in multiphase radial networks," in *Proc. Power Syst. Comput. Conf.*, Aug. 2014, pp. 1–9.

[23] W. Wang and N. Yu, "Chordal conversion based convex iteration algorithm for three-phase optimal power flow problems," *IEEE Trans. Power Syst.*, vol. 33, no. 2, pp. 1603–1613, Mar. 2018.

[24] J. Wang, A. Raza, T. Hong, A. C. Sullberg, F. de León, and Q. Huang, "Analysis of energy savings of CVR including refrigeration loads in distribution systems," *IEEE Trans. Power Del.*, vol. 33, no. 1, pp. 158–168, Feb. 2018.

[25] M. Farivar and S. H. Low, "Branch flow model: Relaxations and convexification: Part I," *IEEE Trans. Power Syst.*, vol. 28, no. 3, pp. 2554–2564, Aug. 2013.

[26] S. H. Low, "Convex relaxation of optimal power flow Part II: Exactness," *IEEE Trans. Control Netw. Syst.*, vol. 1, no. 2, pp. 177–189, Jun. 2014.

[27] W. H. Kersting, *Distibution System Modeling and Analysis*, 3rd ed. Boca Raton, FL, USA: CRC Press, 2012.

[28] A. Bokhari *et al.*, "Experimental determination of the ZIP coefficients for modern residential, commercial, and industrial loads," *IEEE Trans. Power Del.*, vol. 29, no. 3, pp. 1372–1381, Jun. 2014.

[29] K. P. Schneider *et al.*, "Analytic considerations and design basis for the ieee distribution test feeders," *IEEE Trans. Power Syst.*, vol. 33, no. 3, pp. 3181–3188, May 2018.

[30] K. P. Schneider, D. W. Engel, Y. Chen, S. E. Thompson, and R. Pratt, "Modern grid initiative distribution taxonomy," Pacific Northwest Nat. Laboratory, Richland, WA, USA, Tech. Rep. PNNL-18035, Nov. 2008.

[31] A. Nagarajan *et al.*, *Network Reduction Algorithm for Developing Distribution Feeders for Real-Time Simulators: Preprint*, Jun. 2017. [Online]. Available: http://www.osti.gov/scitech/servlets/purl/1364143

Rahul Ranjan Jha (S'16) received the B.Tech. degree from the School of Engineering, Cusat, Kerala, India, in 2012, and the M.Tech degree from the IIT Kanpur, Kanpur, India, in 2015. He is currently working toward the Ph.D. degree at the School of Electrical Engineering and Computer Science, Washington State University, Pullman, WA, USA. His current research interests include optimal power flow, volt-var control and distributed algorithms.

Anamika Dubey (M'16) received the M.S.E and Ph.D. degrees in electrical and computer engineering from the University of Texas at Austin, Austin, TX, USA, in 2012 and 2015, respectively. She is currently an Assistant Professor with the School of Electrical Engineering and Computer Science, Washington State University (WSU), Pullman, WA, USA. Her research focus is on the analysis, operation, and planning of the modern power distribution systems for enhanced service quality and grid resilience. At WSU, her lab focuses on developing new planning and operational tools for the current and future power distribution systems that help in effective integration of distributed energy resources and responsive loads.

Chen-Ching Liu (F'94) received the Ph.D. degree from the University of California, Berkeley, CA, USA. He is currently an American Electric Power Professor and the Director of Power and Energy Center, Virginia Tech, Blacksburg, VA, USA. He is also Research Professor at Washington State University, Pullman, WA, and Visiting Professor at University College Dublin, Ireland. He received the IEEE PES Outstanding Power Engineering Educator Award and Doctor Honoris Causa from Polytechnic University of Bucharest, Bucharest, Romania. He chaired the IEEE PES Technical Committee on Power System Analysis, Computing, and Economics. He is a member of the Washington State Academy of Sciences.

Kevin P. Schneider (S'00–M'06–SM'08) received the B.S. degree in physics and the M.S. and Ph.D. degrees in electrical engineering from the University of Washington, Seattle, WA, USA. He is currently a Chief Engineer at the Pacific Northwest National Laboratory, working at the Seattle Research Center, Seattle, WA. His main areas of research are distribution system analysis and power system operations. He is an Adjunct Faculty member at Washington State University, an Affiliate Associate Professor at the University of Washington, and a licensed Professional Engineer in Washington State. He is the Past Chair of the Power & Energy Society Distribution System Analysis Sub-Committee and the current Chair of the Analytic Methods for Power Systems Committee.